

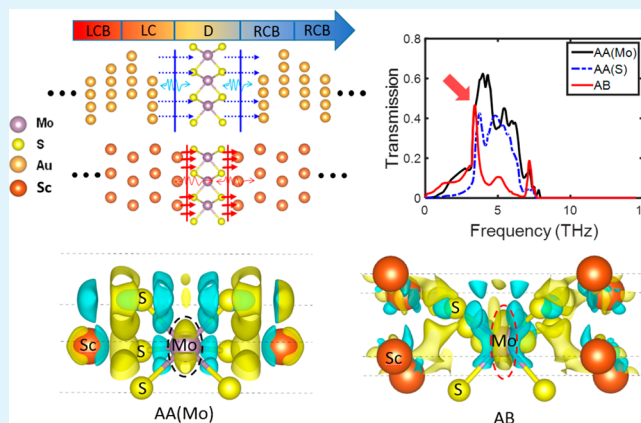
The Role of Interfacial Electronic Properties on Phonon Transport in Two-Dimensional MoS₂ on Metal Substrates

Zhequan Yan,[†] Liang Chen,[‡] Mina Yoon,[§] and Satish Kumar^{*,†}[†]G.W. Woodruff School of Mechanical Engineering, Georgia Institute of Technology, Atlanta, Georgia 30332, United States[‡]School of Energy and Power Engineering, Xi'an Jiaotong University, Xi'an, Shaanxi, P. R. China[§]Center for Nanophase Materials Sciences, Oak Ridge National Laboratory, Oak Ridge, Tennessee 37831, United States

Supporting Information

ABSTRACT: We investigate the role of interfacial electronic properties on the phonon transport in two-dimensional MoS₂ adsorbed on metal substrates (Au and Sc) using first-principles density functional theory and the atomistic Green's function method. Our study reveals that the different degree of orbital hybridization and electronic charge distribution between MoS₂ and metal substrates play a significant role in determining the overall phonon–phonon coupling and phonon transmission. The charge transfer caused by the adsorption of MoS₂ on Sc substrate can significantly weaken the Mo–S bond strength and change the phonon properties of MoS₂, which result in a significant change in thermal boundary conductance (TBC) from one lattice-stacking configuration to another for same metallic substrate. In a lattice-stacking configuration of MoS₂/Sc, weakening of the Mo–S bond strength due to charge redistribution results in decrease in the force constant between Mo and S atoms and substantial redistribution of phonon density of states to low-frequency region which affects overall phonon transmission leading to 60% decrease in TBC compared to another configuration of MoS₂/Sc. Strong chemical coupling between MoS₂ and the Sc substrate leads to a significantly (~19 times) higher TBC than that of the weakly bound MoS₂/Au system. Our findings demonstrate the inherent connection among the interfacial electronic structure, the phonon distribution, and TBC, which helps us understand the mechanism of phonon transport at the MoS₂/metal interfaces. The results provide insights for the future design of MoS₂-based electronics and a way of enhancing heat dissipation at the interfaces of MoS₂-based nanoelectronic devices.

KEYWORDS: density functional theory, atomistic Green's function, MoS₂/metal interface, electron density, phonon transport, thermal boundary conductance



1. INTRODUCTION

Molybdenum disulfide (MoS₂), as one of the promising two-dimensional (2D) materials, offers an alternative to graphene due to its unique electronic^{1–4} and optical properties.^{5–8} Monolayer MoS₂ can be exfoliated from the bulk MoS₂ crystal as a result of the weak van der Waals interlayer interactions or can be grown on substrates using chemical vapor deposition.^{9,10} The large intrinsic bandgap^{1,4,8} and hexagonal planar lattice make it promising for flexible nanoelectronic applications such as field-effect transistors (FETs) with a high on–off ratio and low power consumption.^{11,12} However, an inefficient heat removal through the interface can become a challenge for the performance and reliability of MoS₂-based nanoelectronic devices, especially due to the low thermal boundary conductance (TBC) at the interface of the MoS₂ and its metal contacts.¹³ Only few studies,¹³ nevertheless, have focused on analyzing thermal transport and predicting TBC at the interface of monolayer MoS₂ and metal substrates.

MoS₂ transistors exhibit very high field effect mobility (184–700 cm² V⁻¹ s⁻¹) using scandium (Sc) as a metal contact.¹⁴ However, in contrast to the electron mobility of bulk MoS₂ crystal, that of monolayer MoS₂ ranges from 0.5 cm²/(V s)^{9,15} to 200 cm²/(V s)¹¹ using myriad types of metal contacts. In addition, the research showed that the band structure of monolayer MoS₂ is also influenced by metal contacts.¹⁶ The carrier mobility of a field-effect transistor is limited by scattering from phonons,¹⁷ which are considered the dominant energy carriers for interfacial thermal transport.^{18,19} Therefore, it is necessary to establish a fundamental understanding of the inherent connection between electronic properties and phonon transport at the interface of monolayer MoS₂ and its metal substrates in order to improve heat dissipation and device

Received: August 23, 2016

Accepted: November 8, 2016

Published: November 8, 2016

performance. Furthermore, the interfacial lattice-stacking configurations significantly influence electronic properties^{20–22} and phonon transmission²³ for graphene-based devices. Our understanding of the effects of lattice stacking on the interface of monolayer MoS₂/metals is far from being completed.

In this article, we use first-principles density functional theory (DFT)²⁴ and the atomistic Green's function (AGF) method to elucidate the physical nature of the inherent connection between electronic structure and phonon properties at the interface of single-layer MoS₂ and its metal substrates. We compare phonon transport at Au and Sc contacts with MoS₂ to investigate the differences in the interfacial spacing and electronic structure, which results in two types of interfaces: physisorption and chemisorption. The strong chemisorbed interaction at the MoS₂/Sc interface results in a value of TBC that is 19 times higher than that of the physisorbed interface of MoS₂/Au. To further illustrate how the electronic structure affects the phonon distribution and thermal transport across the interface, we investigate the effects of the lattice-stacking configurations of MoS₂/Sc on electronic and phononic properties. We examine the three typical lattice-stacking MoS₂/Sc interfaces and find that the charge transfer routines caused by the introduction of a metal substrate can affect the strength of the Mo–S bond, which results in the redistribution of phonon density of states (DOSs) and transmission. The influence of lattice-stacking configurations can result in TBC difference by more than 60% because of changes in the electron structure and the force constants. This study is the first to demonstrate the inherent connection among the interfacial electronic structure, the phonon distribution, and TBC, which provides insights into the future design of MoS₂-based electronics and methods of enhancing heat dissipation at the interfaces of MoS₂-based electronic devices.

2. MODELS AND METHODS

We optimize monolayer MoS₂ and its sandwiched structure with metals (Au, Sc) by the Vienna ab initio simulation package (VASP). A plane-wave basis set and the projector augmented-wave (PAW) method are used with the local density approximation (LDA) exchange–correlation functional.^{25,26} A precise description of the interface properties of metal substrates and MoS₂ might require an inclusion of the long-range dispersion interaction (vdW). However, a proper treatment of vdW into the framework of DFT is not a trivial task, despite it being actively investigated by the DFT community for the past decade.^{27,28} In fact, there is no universal DFT functional with a rigorous vdW correction that works for all types of systems. It is generally accepted in the community that generalized gradient approximation (GGA) to the exchange–correlation functional (without adding any vdW corrections) significantly underestimates vdW interactions, while LDA overestimates them or sometimes closely reproduces optimized structures of high-level functional calculations. Specifically, LDA reveals a very good performance in calculating interlayer distance and force constants;^{16,23,29} thus, it is suitable for calculating interfacial TBC that is highly sensitive to the interlayer structure property. The lattice constants of the single-layer MoS₂ are obtained via structural optimization with the value of 3.12 Å, which is in good agreement with experimental results from the previous studies.^{30,31} In our calculations, we use the in-plane lattice constant of single-layer MoS₂ as the surface lattice constant in the sandwiched systems. The 2 × 2 unit cell of Au (111)

substrate can match the $\sqrt{3} \times \sqrt{3}$ unit cell of MoS₂ with an ~3.9% lattice mismatch, whereas the 1 × 1 unit cell of Sc (0001) has the lattice mismatch below 3.2% with the 1 × 1 unit cell of MoS₂ as illustrated in Figure 1a–d. The most stable

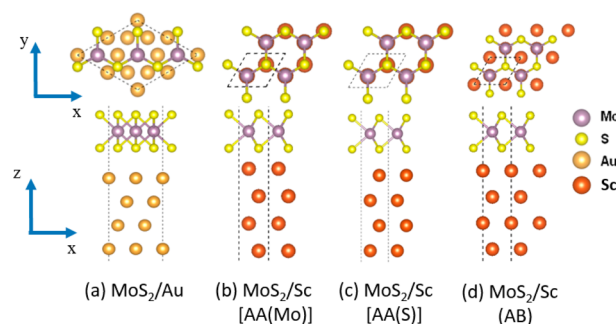


Figure 1. (a) Top and side views of the unit cell of monolayer MoS₂ on the substrate of Au. (b–d) Top and side views of the unit cell of MoS₂/Sc structures with different lattice stacking configurations. (b) For structure AA(Mo), Mo in the parentheses presents that the molybdenum atom is on top of the first-layer Sc atom. (c) For structure AA(S), S in the parentheses presents that the pair of sulfur atoms are on top of the first-layer Sc atom. (d) For structure AB, Mo is on top of the second layer Sc atom while the first layer Sc atom is centered under the MoS₂ hexagonal ring.

contact geometries are obtained by optimizing the structures from various lattice-stacking configurations (Table 1). In the MoS₂/Au(111) system, the three Mo atoms in the unit cell sit above the fcc hollow, hcp hollow, and top sites, respectively, while the three pairs of S atoms are located at the triangle center formed by the fcc, hcp, and top sites. In the MoS₂/Sc(001) system, Mo atom is on top of the first layer Sc atom and the pair of S atoms are on top of the second layer Sc atom. The interfacial distances of the Au/MoS₂/Au and Sc/MoS₂/Sc systems are optimized for the unit cell system with a sampling of 17 × 17 × 1 k-point grids and 25 × 25 × 1 k-point grids, respectively. Using this optimized equilibrium spacing (2.82 Å for MoS₂/Au interface and 1.86 Å for MoS₂/Sc interface), a 3 × 3 supercell of single-layer MoS₂ sandwiched by 4 layers of Au bulks and a 5 × 5 supercell of MoS₂ sandwiched by 4 layers of Sc bulks are assembled for the calculations of second-order interatomic force constants (IFCs) (Figure 2c,d). These supercells contain 369 atoms for the Au/MoS₂/Au system and 275 atoms for the Sc/MoS₂/Sc system with the vacuum region of 16.5 Å. We apply 3 × 3 × 1 k-point grids to sample the Brillouin zone of these supercells. For the supercell system, the kinetic energy cutoff is set to 400 eV. To calculate the IFCs, the displacement length of each atom from its equilibrium position is 0.01 Å.

With the second-order IFCs directly obtained from the DFT calculations, we construct harmonic matrices which provide a reliable prediction of the interatomic interactions for the AGF calculations.^{32,33} The phonon transmission function and TBC at the metal/MoS₂/metal interfaces can be obtained by AGF calculations,^{23,34–36} where single-layer MoS₂ (“device”) is sandwiched between two “contacts” corresponding to the hot and cold thermal reservoirs represented by semi-infinite metal bulks (Figure 2c,d). The heat flux *J* through the system carried by phonons is evaluated by Landauer formalism³⁴

Table 1. Structure Optimization and Thermal Properties of the MoS₂/Metal Interface

structure		interfacial distance (Å)	Sc–S distance at interface (Å)	TBC at room temp (MW/(m ² K))	binding energy per S at interface (eV/atom)
MoS ₂ /Sc	AA(Mo)	1.86	2.58	282	−1.38
	AA(S)	2.58	2.58	172	−0.82
	AB	2.16	2.81	107	−0.82
MoS ₂ /Au		2.82		14.3	−0.20

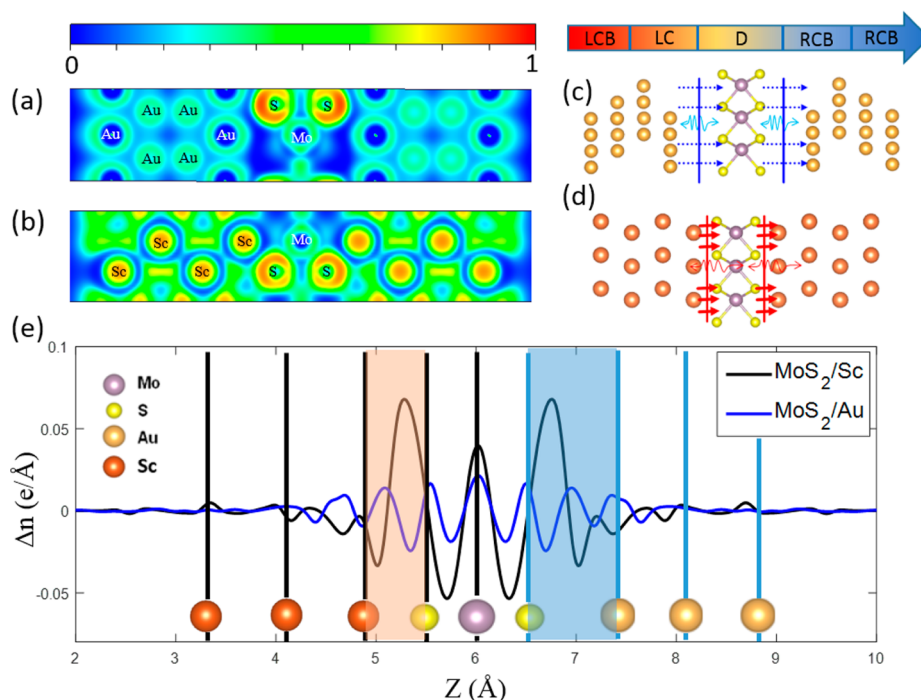


Figure 2. (a, b) Electron localization function (ELF) for the unit cell of (a) MoS₂/Au and (b) MoS₂/Sc. (c, d) Schematic of (c) physisorbed interface of Au/MoS₂/Au and (d) chemisorbed interface of Sc/MoS₂/Sc for the AGF calculations. The interface regions of Sc/MoS₂/Sc and Au/MoS₂/Au are marked as red and blue. The system is divided into a “device” region (D), left contact (LC) and right contact (RC) and two semi-infinite metal bulks, and left contact bulk (LCB) and right contact bulk (RCB) which do not interact with the “device” region. The “device” region only includes the monolayer MoS₂. (e) Plane-averaged electron density difference Δn (per unit cell) along out-of-plane direction showing the charge redistribution at the metal/MoS₂/metal structures. Δn represents the difference in the plane-averaged electron density of the sandwiched structure from metal substrates and free-standing monolayer MoS₂. For comparison, the left part shows only the location of Sc atoms in left half structure of Sc/MoS₂/Sc while the right part shows the location of Au atoms in right half structure of Au/MoS₂/Au.

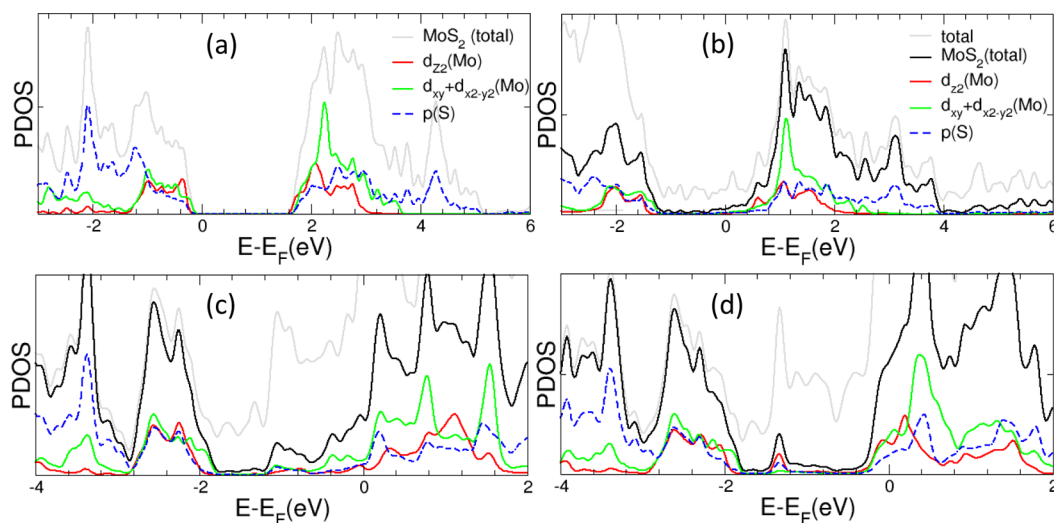


Figure 3. (a–d) Electron PDOS of (a) isolated monolayer MoS₂ (expanded view near the Fermi level is shown in Figure S1), (b) MoS₂/Au, (c) MoS₂/Sc (structure AA(Mo)), and (d) MoS₂/Sc (structure AB).

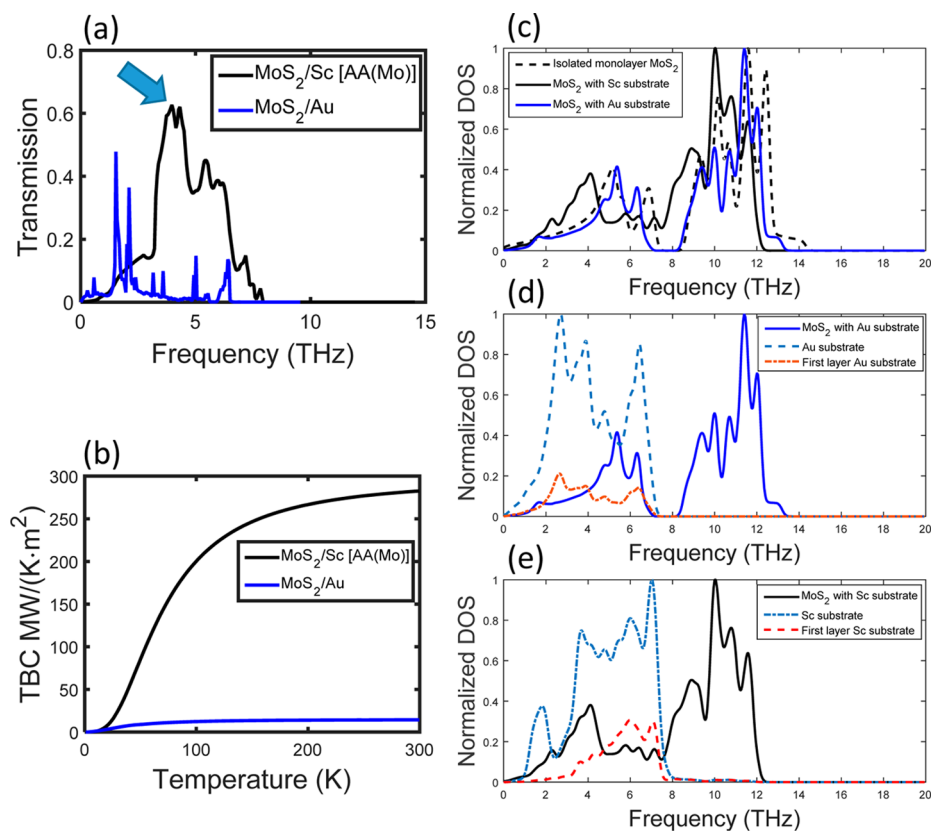


Figure 4. (a) Angular frequency dependent phonon transmission for single layer MoS₂ with Au and Sc substrates. (b) Temperature dependent thermal boundary conductance at interfaces of single layer MoS₂ and metal substrates. (c) Phonon density of states (DOSs) of isolated monolayer MoS₂ and monolayer MoS₂ with different metal substrates. (d) Phonon DOSs of monolayer MoS₂ with Au substrate, Au substrate, and the first layer of Au substrate. (e) Phonon DOSs of monolayer MoS₂ with Sc substrate, Sc substrate, and first layer of Sc substrate.

$$J = \int_0^\infty \int_{\vec{k}_\parallel} \frac{\hbar\omega}{2\pi} [N_L(\omega, T) - N_R(\omega, T)] \Xi(\omega, \vec{k}_\parallel) \frac{d\vec{k}_\parallel}{(2\pi)^2} d\omega \quad (1)$$

More details of the calculation of AGF method can be found in ref 32. The TBC (σ) can be calculated by the definition $\sigma = J/\Delta T$.

3. RESULTS AND DISCUSSION

3.1. Chemisorption or Physisorption? The LDA optimized distances between MoS₂ and the metal substrates are 2.82 Å for Au and 1.86 Å for Sc (for details see Table 1). The significant difference of the interfacial spacing is a good measure of identifying the nature of their interactions; Sc forms a strong bonding with MoS₂ (chemisorption type interaction), while MoS₂ bounds to Au by weak wave function overlaps (physisorption type of interaction). Figure 3a–d presents the partial density of states (PDOS) that reveal their interaction mechanism. For an isolated MoS₂, its conduction band minimum (CBM) is characterized by the d_{z²} orbitals of weakly interacting cations in *xy*-plane, while the valence band maximum (VBM) is contributed by both d_{*xy*} and d_{*x²-y²*} orbitals.³⁷ The CBM and VBM characters are identified in the atomic orbital decomposed PDOS in Figure 3a, where d_{*xy*} + d_{*x²-y²*} states (solid green line) are located at VBM, right below the Fermi level (E_F), and d_{*z²*} states (solid red line) are the frontier states above the Fermi level. The changes of those frontier states upon the interaction with the metal substrates are monitored in Figure 3b–d. Interaction with the metal

substrates overall shifts down MoS₂ states from the isolated states, which indicates charge transfer from the substrates to MoS₂. However, the degree of orbital hybridization between them shows significant differences. For the case of MoS₂/Au system, the dispersion of frontier states below the Fermi level involves the hybridization of Au surface states and s and p_{*z*} orbitals of sulfur, yet the amount of occupation is small (see Figure 3b). This indicates that the weak attractive binding is originated from the weak overlap between the S and Au orbitals and charge transfer to S. On the other hand, for MoS₂ on the Sc substrates, a significant portion of the previous conduction band states become occupied below the Fermi level (see Figure 3c,d), indicating a strong charge transfer from Sc to MoS₂.

Figure 2a,b shows the electron localization function (ELF) contours of the unit cell of MoS₂/Au and MoS₂/Sc. The ELF provides a description of chemical bonds by the probability of finding another same-spin electron in the neighborhood of a reference electron.^{38,39} At the MoS₂/Au interface, electron localization is hardly observed, which means the Au substrate do not have much influence on the electron distribution of the MoS₂ and its interface. We call it a physisorbed interface. However, the strong interaction is indicated in Figure 2b at the interface of MoS₂ and Sc. A strong ELF overlap can be observed at the MoS₂/Sc interface between the S and Sc atoms. Furthermore, the region of high ELF around S is not spherically symmetric and exhibits lobes directed toward the Mo and Sc atoms, which makes the bonding between Mo–S and S–Sc a mixture of ionic and covalent bonds.⁴⁰ We call it chemisorbed interface. To better understand the impact of the metal

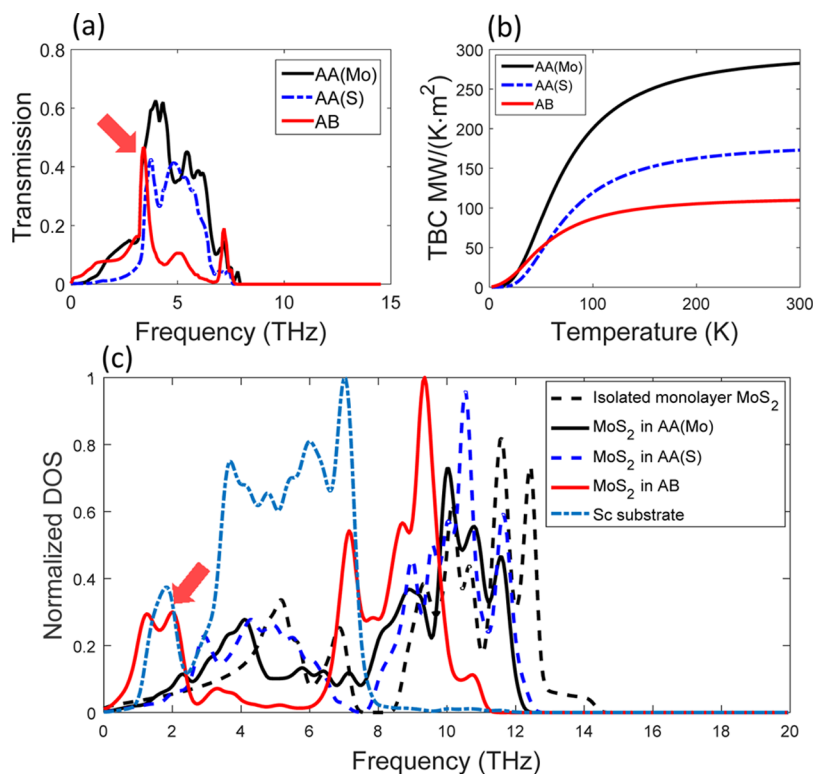


Figure 5. (a) Angular frequency dependent phonon transmission at the interface of MoS₂/Sc for different lattice stacking configurations. (b) Temperature dependent thermal boundary conductance at the interface of MoS₂/Sc for different lattice stacking configurations. (c) Phonon DOSs of isolated monolayer MoS₂, the MoS₂ sandwiched by Sc substrate with different stacking configurations, and the Sc substrate. The red arrow in (c) indicates the phonon redistribution of MoS₂ in AB, which results in the phonon transmission peak in (a) marked by another red arrow.

substrates on the electron redistribution of the interface, the plane-averaged electron density difference Δn was calculated in Figure 2e. The plane-averaged electron density difference Δn is defined as

$$\Delta n(z) = \Delta n_{\text{Sandw}}(z) - \Delta n_{\text{MoS}_2}(z) - \Delta n_{\text{Metal}}(z) \quad (2)$$

where $\Delta n_{\text{Sandw}}(z)$, $\Delta n_{\text{MoS}_2}(z)$, and $\Delta n_{\text{Metal}}(z)$ indicate the plane-averaged densities of the sandwiched structure, free-standing single layer MoS₂, and metals, respectively. The large wavy peak between S and Sc atoms in the red region of Figure 2e indicates that the absolute magnitude of the plane-averaged electron density difference is dramatically higher at the MoS₂/Sc interface than that at the MoS₂/Au interface. It can also be explained by the stronger electron wave function overlap of both MoS₂ and Sc, resulting from the smaller interfacial separation distance.

3.2. Impact of the Interfacial Electron Structure on Phonon Properties. In order to investigate the impact of the interfacial electron structure on the thermal transport of different interfaces, we calculated the phonon transmission at the interfaces using the AGF method (Figure 4a). The TBCs are calculated by the Landauer formula using the transmission function obtained from AGF calculations (Figure 4b). Results show that phonon transmission across the MoS₂/Sc interface is much greater than that of the MoS₂/Au interface (Figure 4a). In addition, Figure 4b shows that the TBC of MoS₂/Sc is 19 times larger than that of MoS₂/Au because of the strong bonding strength at the MoS₂/Sc interface with chemisorbed interactions. To understand the mechanism of the thermal transport of these two different types of interfaces, we calculated the phonon DOSs of MoS₂ and its metal substrates

using IFCs obtained from the DFT calculations^{23,41} in Figure 4c–e. Figure 4c compares the phonon DOSs of isolated monolayer MoS₂, monolayer MoS₂ with Au substrates, and monolayer MoS₂ with Sc substrates. Results indicate that the strong interaction between metal and MoS₂ leads to significant redistribution in the phonon DOSs of MoS₂. After the introduction of the Au substrate, the phonon distribution of MoS₂ does not change much compared with isolated monolayer MoS₂ (Figure 4c). On the other hand, the phonon DOSs of MoS₂ in MoS₂/Sc structure shift to the lower frequencies under the influence of the Sc substrate. It can be explained by the charge transfer among the Mo, S, and Sc atoms, which weakens the Mo–S bond. More details about the impact of charge transfer on the phonon distribution and the force constant will be discussed later. The DOSs shift of MoS₂ in MoS₂/Sc leads to a better match with the DOSs of the Sc bulk, which enhances phonon–phonon coupling and results in a huge transmission peak in Figure 4a around 4 THz.

Furthermore, by comparing Figures 4d and 4e, we find that the significant phonon DOSs mismatch occurs between MoS₂ and Au, which results in low phonon transmission and TBC. In addition, the strong chemisorbed interaction at the MoS₂/Sc interface not only influences the phonon distribution of MoS₂ but also changes the phonon distribution of first-layer Sc atoms. On the other hand, because of the weak physisorbed interaction at the MoS₂/Au interface, the shape of phonon DOSs of first-layer Au atoms near the interface remains similar to that of the Au bulk. These results also explain the different influence on the interface electronic structure and phonon properties caused by the two different types of interfaces.

3.3. MoS₂/Sc Interface with Different Lattice-Stacking Configurations. To further illustrate how interface electronic structure affects the phonon distribution and phonon transport across the interface, we investigate the effects of lattice-stacking configurations of MoS₂/Sc on electronic and phononic properties. Because of the strong chemisorbed interaction across the MoS₂/Sc interface, thermal transport becomes more sensitive to the change of the electron structure.

Three typical lattice-stacking MoS₂/Sc interfaces are examined. Figure 1b–d show the top and side views, in the *x*–*y* plane and *x*–*z* plane, of various lattice-stacking configurations of MoS₂/Sc structures. We distinguish them as AA(Mo), AA(S), and AB. For structure AA(Mo), which has the most stable structure and lowest binding energy (Table 1), Mo in the parentheses presents that the molybdenum atom is on top of the first layer scandium atom. The pair of S atoms is on top of the second layer scandium atom. The MoS₂/Sc structure used in Figure 2 is AA(Mo). For structure AA(S), S in the parentheses presents that the pair of sulfur atoms are on top of the first layer scandium atom. The molybdenum atom is on top of the second layer scandium atom. For structure AB, Mo is on top of the second layer scandium atom while the first layer scandium atom is centered under the MoS₂ hexagonal ring. Structural optimization is conducted by DFT calculation, and results are shown in Table 1. The results show that the TBC at room temperature is in the range of 107–282 MW/(m² K) depending on the stacking configurations in the order of AA(Mo) > AA(S) > AB (Figure 5b). It is clear that structure AA(Mo) has the highest TBC because of its shortest interfacial distance and the best structural stability. However, structure AB has a lower interfacial distance but a lower TBC compared with the structure AA(S). One reason could be the Sc–S distance at the interface of structure AB is larger than that of AA(S). The strong bonding between Sc and S atoms makes the Sc–S distance more important than the actual interfacial gap. However, it cannot explain the significant difference of the shape of the phonon transmission curve in AB compared with the AA(Mo) and AA(S) structures (Figure 5a). To explain this, we calculate the phonon DOSs of MoS₂ in various lattice-stacking structures (Figure 5c). The phonon distribution of MoS₂ in AB reveal a significant difference compared with other structures. For structure AB, there are two large DOSs peak at the low-frequency range under 3 THz and almost no DOSs are between 3 and 6 THz, which leads to a large peak in phonon transmission marked by the red arrow in Figure 5a and the low transmission right after the peak.

3.4. Inherent Connection among Interfacial Electronic Properties, Phonon Transmission, and TBC. To further illustrate the changes in phonon DOSs and transmission, we consider the effect of interfacial lattice-stacking configurations of MoS₂/Sc on their properties. Specifically, we consider two types of stackings, AA and AB, of MoS₂ on Sc. We use AA(Mo) here as a representative of the AA structure. AA(S) is presented in Figures S2 and S3 of the Supporting Information. For the AA(Mo) structure, Mo *d* orbitals form slightly hybridized states with S *p* orbitals, which is shifted down ~1.0 eV below Fermi level, indicating charge transfer from Sc to the Mo *d* and S *p* hybridized states (see Figure 3c). PDOS in Figure 3d reveals that the AB stacking involves a stronger hybridization between Mo *d* and S *p* orbitals, which results in a high intensity in PDOS within ~0.3 eV below the Fermi level. A defect like state located ~1.3 eV below *E_F* is the hybridized state of S *p* and Mo *d_z²* orbitals, where extra charges are transferred. In order to

confirm the understanding from the PDOS, we further visualize changes of charge density upon the adsorption of MoS₂ on Sc. Figure 6a,b shows the charge difference between the MoS₂/Sc

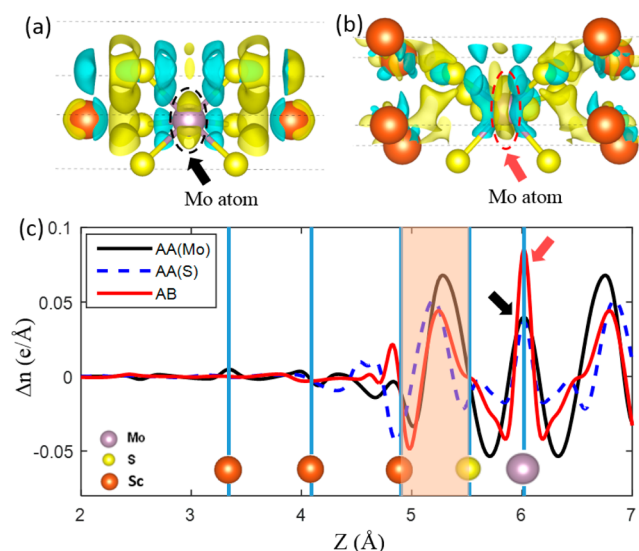


Figure 6. (a, b) Side view of the charge difference between the MoS₂/Sc system and the sum of the isolated MoS₂ and Sc substrate with different stacking configurations: (a) structure AA(Mo) and (b) structure AB. The yellow regions represent the accumulation of electrons, and the blue regions represent the depletion of electrons in the MoS₂/Sc system. Dashed red ellipse in (b) indicates high accumulation of electrons at Mo for structure AB. (c) Plane-averaged electron density difference Δn (per unit cell) along out of plane direction showing the charge redistribution at the Sc/MoS₂/Sc structures with different stacking configurations. The interface of MoS₂/Sc is marked as the shaded region. The peaks pointed by the red and black arrows at 6 Å indicate the charge accumulation around Mo atom which are also marked with dashed ellipse in (a) and (b).

system and the sum of isolated MoS₂ and Sc substrate with the lattice stacking of AA(Mo) and AB. The yellow regions represent the accumulation of electrons, and the blue regions represent the depletion of electrons in the MoS₂/Sc system. In both structures, there exist the electron depletion region between the Mo and S atom, electron accumulation region around the Mo atom, and the region between S and Sc interface. It indicates that the charge transfer has two routines after introducing the Sc substrate. One is from Sc atoms to Mo and S atoms. The other is from the bonded region of Mo–S to Mo atom. Both of the routines will weaken the Mo–S bond^{16,29} which results in the phonon redistribution of MoS₂ in Figure 5c. The intrinsic nature behind the charge transfer and phonon redistribution is the change of the force constant among atoms. More electrons transfer to S–Sc interface in structure AA(Mo) than that in structure AB, which enhances the strength of the bonding between S and Sc. Therefore, the interactions between S and Sc become stronger and lead to a significant increase of the phonon transmission and TBC. On the contrary, the electron transfer to Mo atom in structure AB is larger than that in AA(Mo), which further weakens the strength of the Mo–S bond. The physical connection behind this is the resultant decrease of the force constant between Mo and S atom, which will lower the phonon vibration frequency which keeps more phonons located in the relatively low-frequency region. The phonon DOSs of MoS₂ in structure AB in Figure 5c are the comprehensive results of the weakening of the Mo–S bond. It

can also be demonstrated by Figure 6c. Figure 6c shows the plane-averaged electron density difference along the z direction to differentiate the impact of three different lattice-stacking configurations. It is obvious that AB reveals the largest electron accumulation at the plane of Mo atom compared with the other two structures. On the other hand, AA(Mo) has the largest electron accumulation at the interface between S–Sc, which enhances the interaction between the MoS₂ and Sc substrate leading to the increase of the phonon transmission and TBC. The results are also consistent with our previous conclusions.

4. CONCLUSIONS

In conclusion, we investigate the role of interfacial electronic properties on the phonon transport at the interface of monolayer MoS₂ and metal substrates. We find that different degree of orbital hybridization caused by the introduction of a metal substrate affects the interfacial phonon–phonon coupling and phonon transmission significantly. Strong chemical coupling between MoS₂ and the Sc substrate leads to a 19 times higher TBC than that of the weakly bound MoS₂/Au system. For MoS₂ on the Sc substrates, a strong charge transfer from Sc to MoS₂ can be demonstrated by the significant portion of the previous conduction band states occupied below Fermi level. Furthermore, the effect of interfacial lattice-stacking configurations of MoS₂/Sc leads to a significant redistribution of phonon DOSs and transmission at the interface. The extra charge transfer further weakens the Mo–S bond strength in lattice-stacking configuration of structure AB compared to structure AA(Mo). The resultant decrease in the force constant between Mo and S atoms keeps more phonons located in a low-frequency region which results in a 60% decrease in TBC. The findings in this study demonstrate the inherent connection among the interfacial electronic structure, the phonon distribution, and TBC. Such understanding is very important for nanoengineering of MoS₂/metal interfaces in order to enhance the performance of its electronic devices.

■ ASSOCIATED CONTENT

Supporting Information

The Supporting Information is available free of charge on the ACS Publications website at DOI: 10.1021/acsami.6b10608.

Figure S1: expanded view of PDOS of MoS₂ near the Fermi level; Figure S2: electron PDOS of MoS₂/Sc with the structure of AA(S); Figure S3: the charge difference between the MoS₂/Sc system and the sum of the isolated MoS₂ and Sc substrate with stacking configurations of AA(S) (PDF)

■ AUTHOR INFORMATION

Corresponding Author

*E-mail: satish.kumar@me.gatech.edu (S.K.).

ORCID

Zhequan Yan: 0000-0001-8026-0264

Notes

The authors declare no competing financial interest.

■ ACKNOWLEDGMENTS

This work was partially supported by the National Science Foundation Grant CBET-1236416. Part of this research was conducted at the Center for Nanophase Materials Sciences, which is a DOE Office of Science User Facility and supported

by the ORNL Laboratory Directed Research and Development funding. This research used the resources of the National Energy Research Scientific Computing Center, a DOE Office of Science User Facility supported by the Office of Science of the U.S. Department of Energy under Contract DE-AC02-05CH11231.

■ REFERENCES

- (1) Mak, K. F.; Lee, C.; Hone, J.; Shan, J.; Heinz, T. F. Atomically Thin MoS₂: A New Direct-Gap Semiconductor. *Phys. Rev. Lett.* **2010**, *105* (13), 136805.
- (2) Han, S. W.; Kwon, H.; Kim, S. K.; Ryu, S.; Yun, W. S.; Kim, D. H.; Hwang, J. H.; Kang, J. S.; Baik, J.; Shin, H. J.; Hong, S. C. Band-gap Transition Induced by Interlayer Van der Waals interaction in MoS₂. *Phys. Rev. B: Condens. Matter Mater. Phys.* **2011**, *84* (4), 045409.
- (3) Li, Y.; Zhou, Z.; Zhang, S.; Chen, Z. MoS₂ Nanoribbons: High Stability and Unusual Electronic and Magnetic Properties. *J. Am. Chem. Soc.* **2008**, *130* (49), 16739–16744.
- (4) Huang, Y. L.; Chen, Y.; Zhang, W.; Quek, S. Y.; Chen, C.-H.; Li, L.-J.; Hsu, W.-T.; Chang, W.-H.; Zheng, Y. J.; Chen, W. Bandgap Tunability at Single-layer Molybdenum Disulphide Grain Boundaries. *Nat. Commun.* **2015**, *6*, 6298.
- (5) Zheng, C.; Xu, Z.-Q.; Zhang, Q.; Edmonds, M. T.; Watanabe, K.; Taniguchi, T.; Bao, Q.; Fuhrer, M. S. Profound Effect of Substrate Hydroxylation and Hydration on Electronic and Optical Properties of Monolayer MoS₂. *Nano Lett.* **2015**, *15* (5), 3096–3102.
- (6) Zeng, H.; Dai, J.; Yao, W.; Xiao, D.; Cui, X. Valley Polarization in MoS₂ Monolayers by Optical Pumping. *Nat. Nanotechnol.* **2012**, *7* (8), 490–493.
- (7) Mak, K. F.; He, K.; Shan, J.; Heinz, T. F. Control of Valley Polarization in Monolayer MoS₂ by Optical Helicity. *Nat. Nanotechnol.* **2012**, *7* (8), 494–498.
- (8) Splendiani, A.; Sun, L.; Zhang, Y.; Li, T.; Kim, J.; Chim, C.-Y.; Galli, G.; Wang, F. Emerging Photoluminescence in Monolayer MoS₂. *Nano Lett.* **2010**, *10* (4), 1271–1275.
- (9) Novoselov, K.; Jiang, D.; Schedin, F.; Booth, T.; Khotkevich, V.; Morozov, S.; Geim, A. Two-dimensional Atomic Crystals. *Proc. Natl. Acad. Sci. U. S. A.* **2005**, *102* (30), 10451–10453.
- (10) Lynch, R. W.; Drickamer, H. G. Effect of High Pressure on the Lattice Parameters of Diamond, Graphite, and Hexagonal Boron Nitride. *J. Chem. Phys.* **1966**, *44* (1), 181–184.
- (11) Radisavljevic, B.; Radenovic, A.; Brivio, J.; Giacometti, V.; Kis, A. Single-layer MoS₂ Transistors. *Nat. Nanotechnol.* **2011**, *6* (3), 147–150.
- (12) Qiu, H.; Pan, L.; Yao, Z.; Li, J.; Shi, Y.; Wang, X. Electrical Characterization of Back-gated Bi-layer MoS₂ Field-effect Transistors and the Effect of Ambient on Their Performances. *Appl. Phys. Lett.* **2012**, *100* (12), 123104.
- (13) Mao, R.; Kong, B. D.; Kim, K. W. Thermal Transport Properties of Metal/MoS₂ Interfaces from First Principles. *J. Appl. Phys.* **2014**, *116* (3), 034302.
- (14) Das, S.; Chen, H.-Y.; Penumatcha, A. V.; Appenzeller, J. High Performance Multilayer MoS₂ Transistors with Scandium Contacts. *Nano Lett.* **2012**, *13* (1), 100–105.
- (15) Popov, I.; Seifert, G.; Tománek, D. Designing Electrical Contacts to MoS₂ Monolayers: A Computational Study. *Phys. Rev. Lett.* **2012**, *108* (15), 156802.
- (16) Chen, W.; Santos, E. J.; Zhu, W.; Kaxiras, E.; Zhang, Z. Tuning the Electronic and Chemical Properties of Monolayer MoS₂ Adsorbed on Transition Metal Substrates. *Nano Lett.* **2013**, *13* (2), 509–514.
- (17) Chakraborty, B.; Bera, A.; Muthu, D.; Bhowmick, S.; Waghmare, U. V.; Sood, A. Symmetry-dependent Phonon Renormalization in Monolayer MoS₂ Transistor. *Phys. Rev. B: Condens. Matter Mater. Phys.* **2012**, *85* (16), 161403.
- (18) Koh, Y. K.; Bae, M.-H.; Cahill, D. G.; Pop, E. Heat Conduction across Monolayer and Few-layer Graphenes. *Nano Lett.* **2010**, *10* (11), 4363–4368.

- (19) Chiloyan, V.; Garg, J.; Esfarjani, K.; Chen, G. Transition from Near-field Thermal Radiation to Phonon Heat Conduction at Subnanometre Gaps. *Nat. Commun.* **2015**, *6*, 6755.
- (20) Zhong, X. L.; Amorim, R. G.; Scheicher, R. H.; Pandey, R.; Karna, S. P. Electronic Structure and Quantum Transport Properties of Trilayers Formed from Graphene and Boron Nitride. *Nanoscale* **2012**, *4* (17), 5490–5498.
- (21) Kaloni, T. P.; Cheng, Y. C.; Schwingenschlogl, U. Electronic Structure of Superlattices of Graphene and Hexagonal Boron Nitride. *J. Mater. Chem.* **2012**, *22* (3), 919–922.
- (22) Pashangpour, M.; Bagheri, Z.; Ghaffari, V. A Comparison of Electronic Transport Properties of Graphene with Hexagonal Boron Nitride Substrate and Graphane, A First Principle Study. *Eur. Phys. J. B* **2013**, *86* (6), 1–6.
- (23) Yan, Z.; Chen, L.; Yoon, M.; Kumar, S. Phonon Transport at the Interfaces of Vertically Stacked Graphene and Hexagonal Boron Nitride Heterostructures. *Nanoscale* **2016**, *8* (7), 4037–4046.
- (24) Kresse, G.; Furthmüller, J. Efficiency of Ab-initio Total Energy Calculations for Metals and Semiconductors Using a Plane-wave Basis Set. *Comput. Mater. Sci.* **1996**, *6* (1), 15–50.
- (25) Perdew, J. P. Density-functional Approximation for the Correlation Energy of the Inhomogeneous Electron Gas. *Phys. Rev. B: Condens. Matter Mater. Phys.* **1986**, *33* (12), 8822–8824.
- (26) Kresse, G.; Joubert, D. From Ultrasoft Pseudopotentials to the Projector Augmented-wave Method. *Phys. Rev. B: Condens. Matter Mater. Phys.* **1999**, *59* (3), 1758–1775.
- (27) Klimeš, J.; Bowler, D. R.; Michaelides, A. Van der Waals Density Functionals Applied to Solids. *Phys. Rev. B: Condens. Matter Mater. Phys.* **2011**, *83* (19), 195131.
- (28) Dion, M.; Rydberg, H.; Schröder, E.; Langreth, D. C.; Lundqvist, B. I. Van der Waals Density Functional for General Geometries. *Phys. Rev. Lett.* **2004**, *92* (24), 246401.
- (29) Gong, C.; Colombo, L.; Wallace, R. M.; Cho, K. The Unusual Mechanism of Partial Fermi Level Pinning at Metal–MoS₂ Interfaces. *Nano Lett.* **2014**, *14* (4), 1714–1720.
- (30) Cao, T.; Wang, G.; Han, W.; Ye, H.; Zhu, C.; Shi, J.; Niu, Q.; Tan, P.; Wang, E.; Liu, B. Valley-selective Circular Dichroism of Monolayer Molybdenum Disulphide. *Nat. Commun.* **2012**, *3*, 887.
- (31) Scalise, E.; Houssa, M.; Pourtois, G.; Afanas'ev, V.; Stesmans, A. Strain-induced Semiconductor to Metal Transition in the Two-dimensional Honeycomb Structure of MoS₂. *Nano Res.* **2012**, *5* (1), 43–48.
- (32) Stewart, D. A.; Savic, I.; Mingo, N. First-principles Calculation of the Isotope Effect on Boron Nitride Nanotube Thermal Conductivity. *Nano Lett.* **2008**, *9* (1), 81–84.
- (33) Tian, Z.; Esfarjani, K.; Chen, G. Enhancing Phonon Transmission across a Si/Ge Interface by Atomic Roughness: First-principles Study with the Green's Function Method. *Phys. Rev. B: Condens. Matter Mater. Phys.* **2012**, *86* (23), 235304.
- (34) Zhang, W.; Fisher, T. S.; Mingo, N. Simulation of Interfacial Phonon Transport in Si-Ge Heterostructures Using an Atomistic Green's Function Method. *J. Heat Transfer* **2007**, *129* (4), 483–491.
- (35) Zhang, W.; Fisher, T. S.; Mingo, N. The Atomistic Green's Function Method: An Efficient Simulation Approach for Nanoscale Phonon Transport. *Numer. Heat Transfer, Part B* **2007**, *51* (4), 333–349.
- (36) Chen, L.; Huang, Z.; Kumar, S. Impact of Bonding at Multi-layer Graphene/metal Interfaces on Thermal Boundary Conductance. *RSC Adv.* **2014**, *4* (68), 35852–35861.
- (37) Kang, J.; Tongay, S.; Zhou, J.; Li, J.; Wu, J. Band Offsets and Heterostructures of Two-dimensional Semiconductors. *Appl. Phys. Lett.* **2013**, *102* (1), 012111.
- (38) Savin, A.; Nesper, R.; Wengert, S.; Fässler, T. F. ELF: The Electron Localization Function. *Angew. Chem., Int. Ed. Engl.* **1997**, *36* (17), 1808–1832.
- (39) Silvi, B.; Savin, A. Classification of Chemical Bonds based on Topological Analysis of Electron Localization Functions. *Nature* **1994**, *371* (6499), 683–686.
- (40) Li, Y.; Li, Y.-L.; Araujo, C. M.; Luo, W.; Ahuja, R. Single-layer MoS₂ as an Efficient Photocatalyst. *Catal. Sci. Technol.* **2013**, *3* (9), 2214–2220.
- (41) Li, J.; Yeung, T. C. A.; Kam, C. H. Phonon Transport in Nanowire with Contacts: Size and Doping. *J. Appl. Phys.* **2012**, *111* (9), 094308.